Theory of Current Source-Density Analysis and Determination of Conductivity Tensor for Anuran Cerebellum

CHARLES NICHOLSON AND JOHN A. FREEMAN

Division of Neurobiology, Department of Physiology and Biophysics, University of Iowa, Iowa City, Iowa 52242; and Department of Anatomy, Vanderbilt University, Nashville, Tennessee 37232

INTRACELLULAR electrical recording can yield precise data about information processing within neuronal elements. It is often impossible, however, to make stable intracellular recordings from the neuronal elements of the central nervous system; in such cases it is necessary to use extracellular potentials as indicators of neuronal function. This paper and the subsequent one deal with a method of analyzing extracellular field potentials, known as current source-density (CSD) analysis, which is capable of yielding surprisingly precise information about neuronal activity.

The neuronal elements of the nervous system are embedded within a conductive matrix which constitutes the extracellular medium. The transmembrane currents which flow across the membrane of active neuronal elements establish an ensemble of current sources and sinks with respect to the extracellular medium. This ensemble constitutes a CSD distribution which is a manifestation of events of physiological interest, such as synaptic currents and action currents. The extracellular current flowing between the sources and sinks gives rise to potential differences which are generally referred to as field potentials and which can be monitored with a microelectrode.

Much useful information about neuronal activity may be deduced from inspection of field potentials at selected loci (18). It is, however, a consequence of the physical principle of superposition that potentials generated by sources and sinks add algebraically at any given point. This often makes interpretation ambiguous. In order to resolve such difficulties, recourse must usually be made to anatomical information about the spatial distribution of probable current-generating regions within the cell. Since field potentials may not be highly localized within a particular region, even careful anatomical studies cannot guarantee acceptable resolution of the sites of sources and sinks in all cases.

For the above reasons it is highly desirable to have a direct method of computing the temporal and spatial distribution of current sources and sinks within the tissue of the central nervous system during neuronal activity. Pitts (25) introduced CSD analysis and the technique has been implemented subsequently in various forms (3, 5–7, 10, 12, 17, 29), but the theoretical and practical basis of the method has remained rather undefined. It is the purpose of this paper and the following one (2) to put CSD analysis on a more reliable basis and thus encourage its use; application to the anuran cerebellum will be used as a demonstration of the technique.

At the outset it is important to distinguish between the current source density (CSD) and current flow density. Confusion arises since both are often referred to simply as current densities. The CSD is a scalar quantity which measures the amplitude of the source or sink of current at a given point. In the present context a source is equivalent to current being injected into the extracellular medium from within a neuronal element and a sink equivalent to current being absorbed from the medium into a

Received for publication April 1, 1974.

neuronal element (21, 22). The CSD is related to the second spatial derivatives of the potential. The current flow density is a vector quantity which measures the amplitude and direction of current flowing through a given point in the extracellular medium. The current flow density is related to the first spatial derivatives of the potential. Current flow density has been used recently as a tool for cerebellar analysis (13), however since it does not directly indicate sources and sinks, its interpretation is difficult.

This paper will discuss the theory of CSD analysis and the measurement of the conductivity tensor. The second paper will deal with the practical implementation of CSD analysis.

METHODS

Experimental preparation

Experiments were performed on adult bullfrogs *(Rana catesbeiana)* and toads *(Bufo marinus)* weighing 400–600 g. Frogs were immobilized with *d*-tubocurarine (4 mg/kg) and xylocaine applied at pressure points. Toads were immobilized by succinylcholine chloride (0.1 mg/kg) or by epidural spinal anesthesia with hypertonic 1% xylocaine. Both were kept moist by oxygenated H_2O and were artificially respirated. The cerebellum was exposed and micropipettes (5–10 MΩ at 1,000 Hz) filled with 4 M NaCl were used to record field potentials and to inject curent. The tips were beveled with an air-bearing grindstone (34) for ease of penetration. Potentials were recorded using a multichannel high-input impedance capacity-compensated FET headstage and associated conventional electronics (Fig. 1). Computations were performed with a PDP-12 computer. Stimuli were delivered by a multichannel digital stimulator (F. C. Haer), and stimulus artifacts were electronically suppressed (1). Electrode positions were determined by use of a three-dimensional micrometer accurate to within ±2 μm (Narishige ME-7).

Measurement of conductivity tensor

The relationship between the potential $\psi(x)$, produced at the point $\mathbf{x} = (x, y, z)$ by a point source of magnitude I at the origin of an infinite, homogeneous volume conductor having principal conductivities $\sigma_x, \sigma_y, \sigma_z$ is given by (3, 19, 23),

$$\psi(x, y, z) = I/4\pi[\sigma_y\sigma_z x^2 + \sigma_z\sigma_x y^2 + \sigma_x\sigma_y z^2]^{\frac{1}{2}} \quad (1)$$

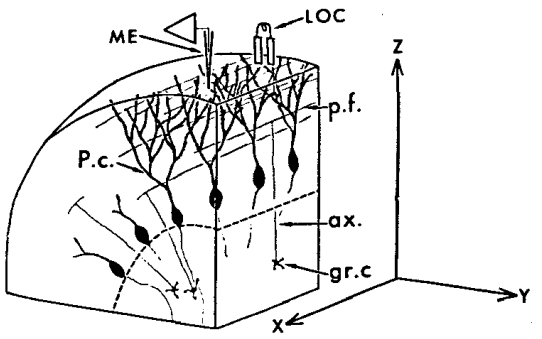

FIG. 1. Alignment of rectangular axes with intrinsic cerebellar geometry and set up for local stimulation. *x* and *y* axes are parallel to cerebellar surface with *x* axis aligned with parallel fibers (pf). *z* axis is perpendicular to cerebellar surface and thus aligned with vertical axis of Purkinje cells (Pc) and ascending branch of granule cell (grc) axons which bifurcate to give rise to the pf. A local electrode (LOC) stimulates pf which synaptically excite the Pc. The resulting field potentials are recorded by one or more microelectrodes (ME) and appropriate amplifiers.

For a semi-infinite medium, with the origin lying in the surface, the right-hand side of *equation 1* will be doubled, since all the current is restricted to the semi-infinite volume. This is the case considered here where the current electrode was a micropipette placed just beneath the pial surface of the cerebellum, while the surface itself was covered with an insulating layer of mineral oil. A second micropipette was then used to record the potential generated at a set of four points (x_1, y_1, z_1), (x_2, y_1, z_1), (x_1, y_2, z_1), and (x_1, y_1, z_2). *x* and *y* coordinates run parallel to the plane of the surface, with the *x* axis aligned with the parallel fibers; the *z* axis is perpendicular to the surface (see Fig. 1). In a previous study (3) it was found that the measurement of potential distribution in response to a constant current, and subsequent calculation of conductivity component, was very sensitive to error in potential measurement and electrode position.[1] In the present work a new method of measuring conductivities was employed which was less sensitive to errors. The method consisted of using a feedback circuit (Fig. 2) to produce an extracellular voltage clamp and then measuring the currents required to produce a voltage ψ_s equal to the command voltage ψ_c at the four observation points. If the currents are I_1 for (x_1, y_1, z_1), I_2 for (x_2, y_1, z_1), I_3 for (x_1, y_2, z_1), and I_4 for (x_1, y_1, z_2), then

[1] Note that in ref 3 the factor in the denominator of *equation 4* should be 4π and *equation 4* should be multiplied by 2 to yield the formulas for the semi-infinite cases which thus should have factors of 2π in their denominators.

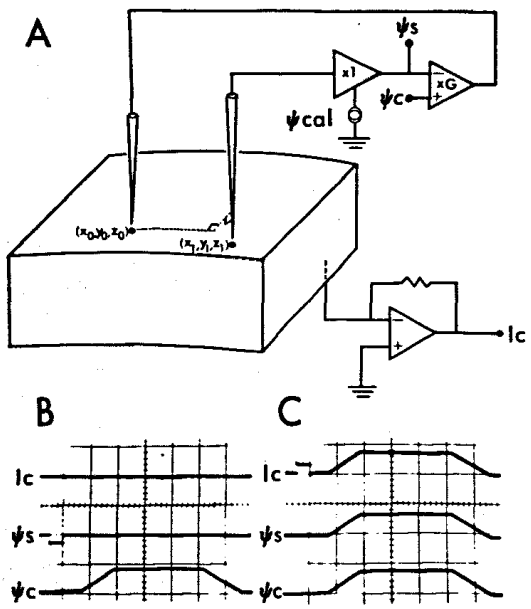

FIG. 2. Extracellular voltage-clamp technique used to measure tissue conductivity. *A:* experimental set up. Potential (ψ_s) is measured at (x_1, y_1, z_1) via unity-gain high-impedance amplifier. This signal is fed to variable-gain (G) clamp-control amplifier which also receives command voltage pulse ψc. The control amplifier injects current through a second electrode at (x_0, y_0, z_0) until ψs = ψc. The injected current, Ic, is measured via a current monitor in the ground lead to the preparation. *B, C:* typical waveforms recorded with clamp turned off and on, respectively, showing adequacy of clamp. Voltage calibration pulse (ψcal): 2 ms, 1 mV. Current calibration pulse: 2 ms, 0.5×10^{-8} A.

using *equation 1* and multiplying it by two for the semi-infinite case it can be shown that:

$$\sigma_x = \frac{1}{2\pi\psi_s}\left\{\frac{(I_1^2 - I_3^2)(I_1^2 - I_4^2)(x_1^2 - x_2^2)}{(I_1^2 - I_2^2)(y_1^2 - y_2^2)(z_1^2 - z_2^2)}\right\}^{\frac{1}{2}}$$

$$\sigma_y = \frac{1}{2\pi\psi_s}\left\{\frac{(I_1^2 - I_4^2)(I_1^2 - I_2^2)(y_1^2 - y_2^2)}{(I_1^2 - I_3^2)(z_1^2 - z_2^2)(x_1^2 - x_2^2)}\right\}^{\frac{1}{2}}$$

$$\sigma_z = \frac{1}{2\pi\psi_s}\left\{\frac{(I_1^2 - I_2^2)(I_1^2 - I_3^2)(z_1^2 - z_2^2)}{(I_1^2 - I_4^2)(x_1^2 - x_2^2)(y_1^2 - y_2^2)}\right\}^{\frac{1}{2}} \quad (2)$$

Conductivities were measured for a set of points, spaced 50 μm apart. For each measurement a trapezoidal command voltage was used in the clamp (Fig. 2*B, C*) and the current injected for 50 repetitions of the command voltage was averaged and stored in the computer.

The majority of the signal energy above 3,000 Hz is electrode noise, so that the signals were band limited to 0–3,000 Hz. Use of the trapezoidal command pulse avoided problems of phase shift and clamp oscillation. The rise and fall time of the trapezoidal pulse was varied in order to study the frequency dependence of tissue conductivity. The maximum value of current injected did not exceed 0.8×10^{-7} A; in control experiments currents of this strength did not produce any detectable electrical response at the recording electrodes or any alteration of the excitability of parallel fibers to stimulation of the folial surface.

Potential dependence of conductivity

A precise reference sinusoidal current (0.5×10^{-7} A) was injected via a micropipette (4 M NaCl, 5 MΩ) into the molecular layer of the cerebellar cortex (Fig. 3). The potential produced by this current was recorded with another micropipette 100 μm away on the same beam of parallel fibers, and fed to a frequency-selective amplifier (P. A. R. model 220). This amplifier was adjusted so that *a*) the amplitude of the tuned resonance filter output varied linearly with changes in the amplitude of the sinusoidal signal, and was independent of potentials generated by the cerebellum at other frequencies, and *b*) the notch filter removed the reference sinusoid. Since the injected current was constant (i.e., not affected by changes in resistance of the current-injecting electrode), any change in the tuned resonance output V_N of the lock-in amplifier reflects a change in conductivity given by $V_N = i(z_a + z_b)/(z_a + z_b + z_x)$ (see Fig. 3). The system was calibrated using a transistor circuit whose equivalent impedance could be varied; the system was capable of detecting impedance changes of less than 0.06%.

THEORY AND EXPERIMENTAL RESULTS

Pitts (25) suggested that the relationship between the CSD and extracellular field

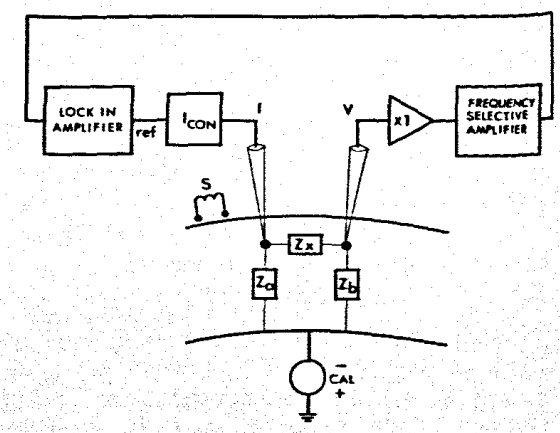

FIG. 3. Technique used to measure voltage dependence of conductivity using a lock-in amplifier. Explained in text.

potentials should be described by Poisson's equation. Later studies (3, 26) have demonstrated that the flow of current in extracellular space satisfies quasistatic conditions and that the extracellular medium obeys ohm's law at the frequencies encountered during normal physiological activity. Data to be presented later in this paper confirm these conclusions.

The relationship between the field potential ϕ at the point $\mathbf{x} \equiv x, y, z$ and the CSD, $I_m(\mathbf{x})$, has been derived elsewhere (21, 22) for quasistatic conditions. The elements of the derivation are that a given CSD represents a continuous spatial distribution of sources and sinks which give rise to a three-dimensional current flow $\mathbf{J}(\mathbf{x})$. Continuity considerations relate $\mathbf{J}$ and I_m through a divergence operation

$$\nabla \cdot \mathbf{J} = I_m \tag{3}$$

By Ohm's law the current flow is a function of the electric intensity $\mathbf{E}(\mathbf{x})$ and the conductivity tensor $\sigma(\mathbf{x})$:

$$\sigma \mathbf{E} = \mathbf{J} \tag{4}$$

Magnetic effects can be neglected, hence the electrodynamic field is irrotational ($\nabla \times \mathbf{E} = 0$) (20). $\mathbf{E}$ thus may be represented by the gradient of a scalar quantity: the field potential, $\phi(\mathbf{x})$

$$\mathbf{E} = -\nabla \phi \tag{5}$$

From *equations 3–5*

$$\nabla \sigma \cdot \nabla \phi = -I_m \tag{6}$$

Note the difference between the CSD, I_m, which is a scalar, and the current flow density vector $\mathbf{J}$. The CSD provides the sources and sinks for the current flow, which in turn generates potential differences by flowing through the ohmic medium of the tissue. The relationships between I_m, $\mathbf{J}$, and ϕ are illustrated in Fig. 4 for observations along the axis of symmetry of a simple cylindrical ensemble of sources and sinks described in APPENDIX II. The field potential does not mirror the CSD, positive and negative field potentials exist at points where the CSD is zero, and the reversal point of the field potential does not occur at the zero crossing of the CSD. Figure 4 also shows that the reversal points of the current flow component J_z do not occur at well-defined points relative to the distributed CSD.

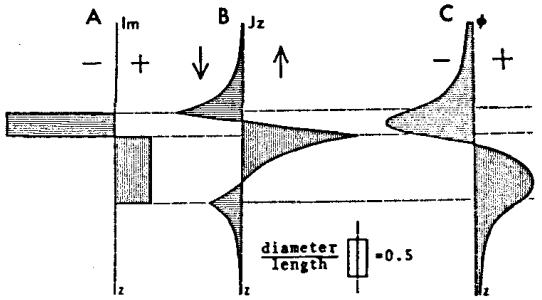

FIG. 4. Relationships between CSD, current flow, and field potential in simple case. Graphs are computed for cylindrical model (APPENDIX II) having diameter-to-length ratio of 0.5 embedded within an infinite medium of finite conductivity. Computation for points on z axis (axis of cylindrical symmetry) only. The CSD (I_m) shown in *A* gives rise to a current flow, the z component of which is shown in *B* (J_z). Downward current flow shown to left of axis, upward to the right. The current flow establishes the field potentials (ϕ) shown in *C*. Polarity of I_m and ϕ as indicated. See APPENDIX II for details of model. All graphs in arbitrary units.

Equation 6 is independent of any given coordinate system and thus is the most general expression of the relationship between the field potential and CSD. When the tensor σ has components which are not space dependent, *equation 6* may be transformed into Poisson's equation (21).

The CSD, I_m, may be related to the current flowing normally across the membrane of a neuronal element by the equation

$$\int_V I_m d^3x = \sum_{i=1}^{n} \int_{M_i} \mathbf{J}_m \cdot d\mathbf{s} \tag{7}$$

Where the volume V contains n neuronal elements, each with surface M_i and surface elements ds across which a current $\mathbf{J}_m$ flows.

This equation defines I_m as a smoothed-out continuous source density and is discussed in more detail by Nicholson (21). When the neuronal geometry has a high degree of symmetry, *equation 7* may yield a very simple relationship between the CSD and the transmembrane current. For example, when the neuronal elements are core conductors passing normally with a density $\nu(\mathbf{x})$ per unit area, through a given plane, then

$$I_m = \nu i_m \tag{8}$$

where $i_m(\mathbf{x})$ is the transmembrane current as defined by cable theory (see APPENDIX I

for details). In most cases it is sufficient to compute I_m without discussing its precise relationship to the individual elements.

Before expressing *equation 6* in an appropriate coordinate system we shall illustrate the differences between the CSD and the field potential.

Current source densities and field potentials compared

The inherent accuracy of the current source-density technique is shown by a set of experiments illustrated in Fig. 5. Two pairs of micropipettes were used to inject

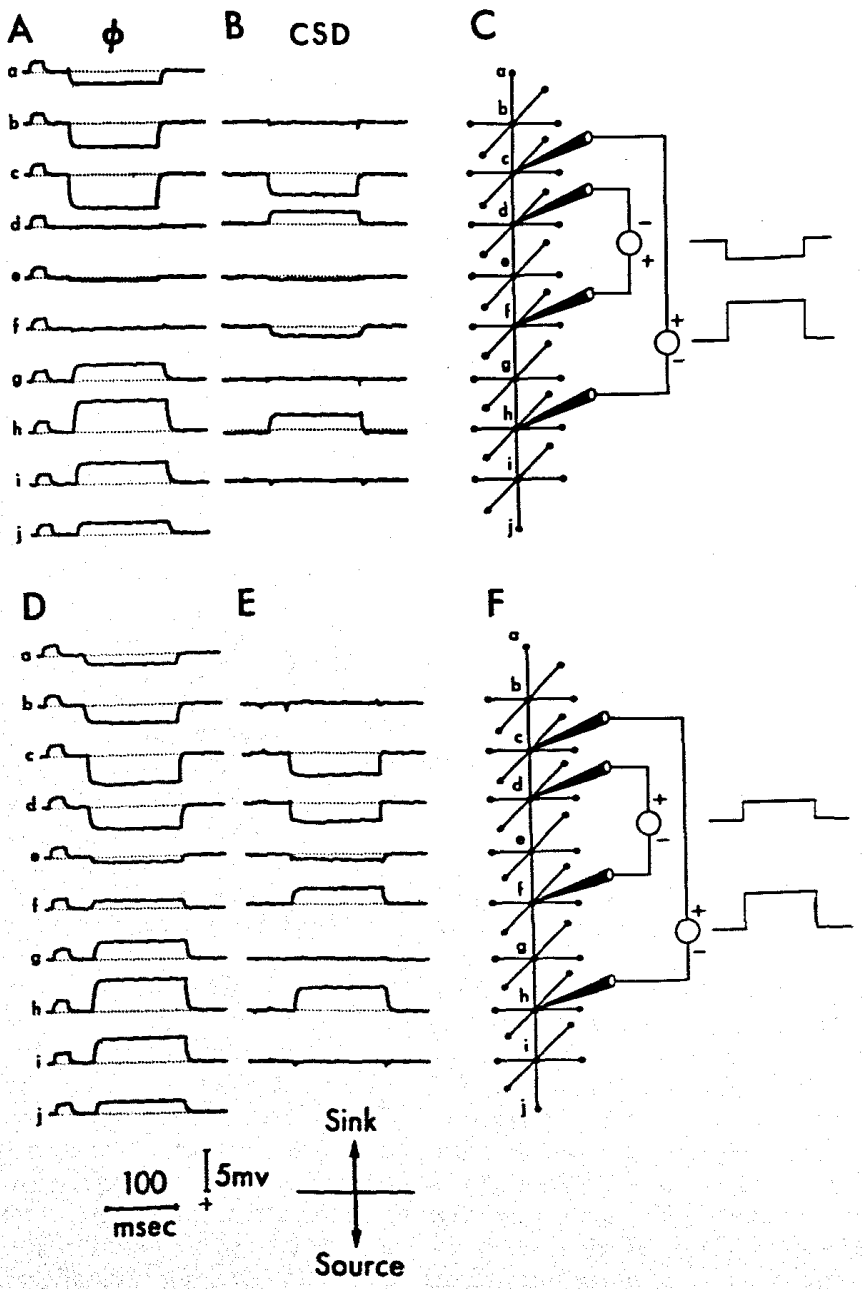

FIG. 5. Experimental comparison of accuracy of field potential and CSD analysis. Two pairs of current-injecting microelectrodes were positioned to provide sources and sinks of current at known locations (*C* and *F*). Note the opposite polarity of the inner pair in *C* and *F*. *A* and *D:* laminar field potentials recorded at the center track. *B* and *E:* CSD records at points corresponding to those in *A* and *D*. The correct location and polarity of the sources and sinks is clearly revealed by the CSD but not the field-potential waveforms. Note that the field potentials at locations d and f in *A* are essentially zero, even though a current sink and source, shown in the CSD records, were located at those locations.

known current sources and sinks into the cerebellum. The locations of the current-injecting electrodes are shown in Fig. 5*C* and *F*, the outer pair enclosing the inner pair. Field potentials were measured at regularly spaced points 50 μm apart in a three-dimensional lattice beginning with the top point just beneath the surface. In both sets of records the outer pair of micropipettes provided a superficial positivity (source) to a deep negativity (sink). In the top set of records the inner pair of micropipettes provided simultaneously a second smaller superficial negativity and deeper positivity. The polarity of this inner pair of electrodes was reversed in the bottom set of records. The corresponding laminar field potentials and CSD waveforms are shown in the left-hand and middle columns, respectively. Note that the field potentials for both configurations of sources and sinks (Fig. 5*A* and *D*) are quite similar even though the current pulses are not, and consist of a set of superficial positive potentials which increase with depth and then reverse to a deeper negativity. It is readily apparent that neither the amplitude nor the reversal point of the field potentials indicate the correct location of the current sources and sinks, whereas these are quite accurately localized by the CSD analysis (Fig. 5*B* and *E*).

The difference in spatial resolution between the CSD and field potential can be accounted for by considering the implications inherent in the formalism of *equation 6*. When this equation is solved in a suitable coordinate system, the potential at the point x may be expressed as a weighted integral of the CSD, I_m, i.e.:

$$\phi(x) = \int_V G(x, x')\, I_m(x') d^3x' \qquad (9)$$

where the volume integral is taken over the appropriate region of neuronal tissue (21). The weighting function G(x,x') depends on anatomical paramaters such as the size of the neuronal population, symmetry properties, and value of the conductivity tensor (21). If the weighting function is sharply localized around the observation point the field potential will be a fairly good measure of the local CSD. On the other hand, if the weighting function is relatively flat, the recorded potential will tend to be an average of the CSD over a large volume: in the limit this average will be zero since the algebraic sum of all sources and sinks must be zero. Thus, without further analysis, the field potential does not provide good spatial resolution of the CSD.

Expression for CSD in rectangular Cartesian coordinates

As a first step toward making practical measurements based on *equation 6* it is necessary to express it in a particular coordinate system. The rectangular Cartesian system is the simplest and some regions of the brain, particularly areas of the cerebellum, have an intrinsic rectangular system.

Equation 6 is represented in rectangular coordinates by:

$$\sum_{i=1}^{3} \sum_{j=1}^{3} \frac{\partial}{\partial x_i} \sigma_{ij} \frac{\partial}{\partial x_j} \phi = -I_m \qquad (10)$$

where $x_1 \equiv x$, $x_2 \equiv y$, and $x_3 \equiv z$.

Since the conductivity tensor is symmetric (14), it may always be reduced to its three principal components by a suitable coordinate rotation to the principal axes (20). In tissues which have an intrinsic rectangular geometry, such as the cerebellum, these axes may be regarded as the principal axes and by making measurements with respect to them, one need only consider conductivity components $\sigma_{11} \equiv \sigma_x$, $\sigma_{22} \equiv \sigma_y$, and $\sigma_{33} \equiv \sigma_z$ (13). σ_x, σ_y, and σ_z may also be functions of space, that is the tissue may be inhomogeneous as well as anisotropic, in which case their first partial derivatives will appear in *equation 10*.

It is worthwhile at this point to define our usage of the terms anisotropic and inhomogeneous. By anisotropic we mean that the conductivity is different in different directions as defined by the coordinate system. Mathematically this means that the tensor has at least two nonequal principal components. When the medium is isotropic, all principal components are equal and may be represented by a scalar (zero-order tentor). Inhomogeneity means that the conductivity is a function of spatial location and will differ from place to place; this means that there are points for which

$\partial\sigma_{ii}/\partial x_i \neq 0$. Anisotropy and inhomogeneity are independent properties and the existence of one does not imply the existence of the other.

If σ is not a function of space and measurements are made in the principal axes, *equation 10* may be written as

$$\sigma_x \frac{\partial^2\phi}{\partial x^2} + \sigma_y \frac{\partial^2\phi}{\partial y^2} + \sigma_z \frac{\partial^2\phi}{\partial z^2} = -I_m \qquad (11)$$

It will be shown below that this equation is appropriate for the anuran cerebellum. The more complex case of rotated axes and spatially dependent conductivities is treated in APPENDIX II.

Before describing the results of measurements of the conductivity tensor and their implications for the validity of *equation 11*, we shall discuss the necessity of using all the components of the second spatial derivative in order to estimate the CSD.

Minimum number of dimensions needed for accurate CSD analysis

Equation 6 implies that measurements of second spatial derivatives must be made in three dimensions. Some studies (6, 7) have relied on one-dimensional analysis, and one may ask what type of error is introduced by relying on measurements along a single axis. We studied this with the simple theoretical model described in APPENDIX II. This consisted of a cylindrical distribution of sources and sinks having the amplitudes illustrated in Figs. 4 and 6. The ratio of the diameter to length of the cylinder was varied and the single second derivative $\partial^2\phi/\partial z^2$ was computed for the z axis (axis of symmetry). Figure 6 shows that when the population is narrow, the second derivative in the z direction does not accurately represent the CSD. As the diameter of the population increases, the resemblance between the single second derivative and the CSD increases, but a large, synchronous ensemble is necessary in order to obtain close similarity. Thus in general, it is necessary to measure all three second derivatives, and our experimental measurements (2) have shown that this is necessary in the anuran cerebellum. The use of all the components of the second derivate necessitates the measurement of the three principal components

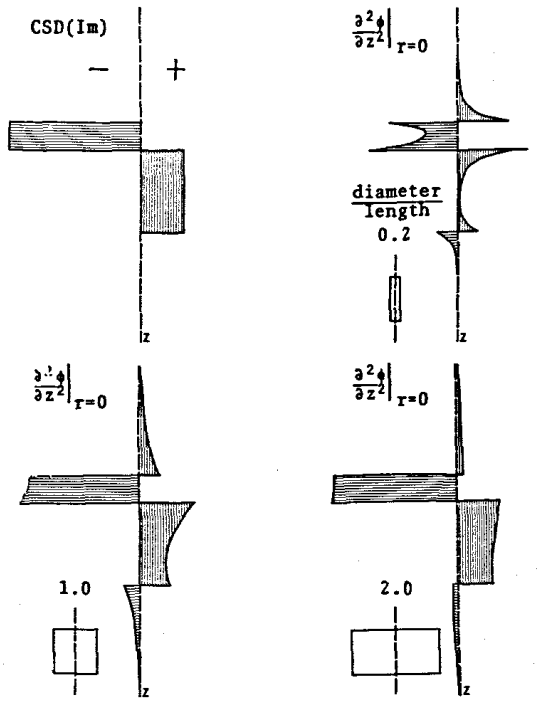

FIG. 6. Second derivatives along z axis as estimate of CSD for simple model. Ideal CSD (I_m) distribution for cylindrical model (APPENDIX II) shown at upper left. Other illustrations show $\partial^2\phi/\partial z^2$, computed for cylinder axis ($r = 0$), for increasing diameter to length ratios, $\partial^2\phi/\partial z^2$ only begins to approximate I_m for large-diameter populations. See also Fig. 4. Figures in arbitrary units, positive to right of vertical axis, negative to left.

of the conductivity tensor and the possible spatial and potential dependence.

Determination of conductivity tensor

PRINCIPAL COMPONENTS. These measurements were made on frog and toad cerebella using the extracellular voltage clamp technique described in METHODS.

Comparative values of the principal components of the conductivity tensor are shown in Fig. 7; the average value of conductivity and the range of values (vertical lines) from five animals of each species are plotted at increasing depths beneath the folial surface. Both frog and toad cerebella are anisotropic, confirming earlier measurements (3). The conductivity at a given location in each axis correlates well with the relative local abundance of core conductors oriented in the same axis. For both frog and toad, the computed values of the conductivity components in the direction of the parallel fibers are maximum in the re-

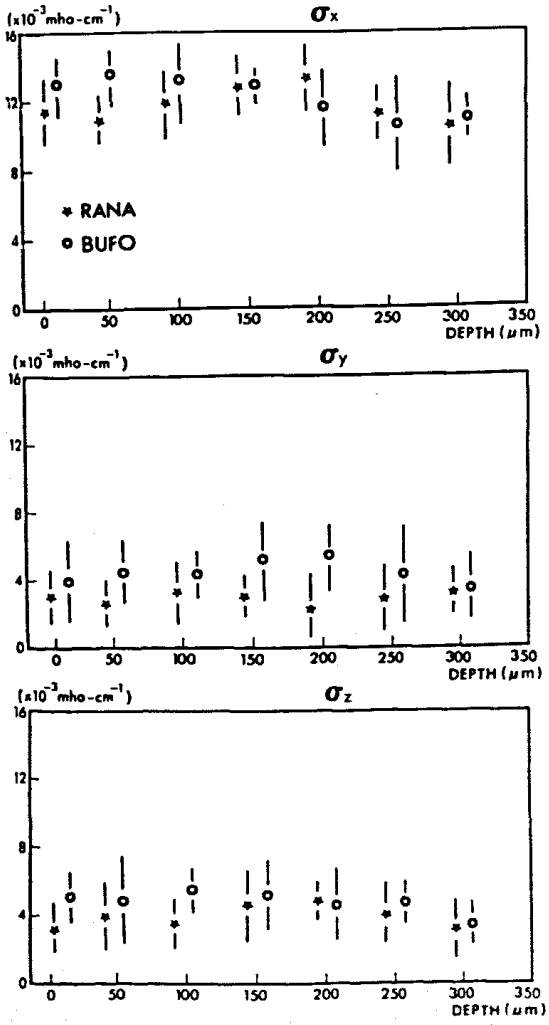

FIG. 7. Experimentally obtained values of components of conductivity tensor in the frog (*Rana*) and toad (*Bufo*) cerebellum as a function of depth (z). Symbols indicate mean, bars indicate standard deviations.

gion of parallel fibers, and decrease slightly below it (see Fig. 6*C*). The conductivity components in the directions transverse to this but parallel with the surface remain fairly low throughout the cerebellum, which correlates with the paucity of core conductors oriented in this direction. The values of the conductivity components normal to the surface remains fairly uniform from the surface downward, decreasing slightly below the level of the Purkinje cell somata. The dependence of conductivity on frequency was negligible for command pulse rise times up to 0.5 ms (2,000 Hz). We assume that most of the energy in physiological signals of interest lies well below this value.

SPATIAL CONDUCTIVITY GRADIENTS. The anatomical symmetry of the anuran cerebellar anatomy (8, 9) suggests that one should expect to find a conductivity gradient in the *z* direction only. The homogeneity of conductivity in the *x-y* plane is demonstrated by the fact that random entries into the cerebella of five species of each chosen animal yielded similar results. Figure 7 shows that even in the *z* direction the gradients of conductivity are sufficiently small to be neglected down to a depth of 300 μm, hence the three principal values of conductivity may be taken as constant. The values and their standard deviations are given in Table 1.

The values for *R. catesbeiana* are in agreement with those reported previously (3).

POTENTIAL DEPENDENCE OF CONDUCTIVITY. Calculations of CSD are based on the assumption that the medium is ohmic; that is, the conductivity is not potential dependent. In the present context this implies that the conductivity should remain constant during the neuronal activity generated by typical cerebellar stimulation. To verify this we stimulated the cerebellar surface locally (16) and used a lock-in amplifier to detect conductivity changes, as detailed in the METHODS section. Results obtained with this technique are shown in Fig. 8. Figure 8*C* is the headstage output, consisting of the parallel fiber field potential produced by local surface stimulation, superimposed on the 1,000-Hz reference excitation signal from the current-injecting electrode. The field potential is clearly seen in the resonance output of the lock-in amplifier (Fig. 8*A*). A minute (less than 1%) change in conductivity during the peak of the parallel fiber volley is seen in the tuned resonance output (Fig. 8*B*), shown with the gain increased 100 times. In five such experiments

TABLE 1. *Conductivity values of frog and toad cerebella*

Component of Conductivity	Conductivity, mho·cm−1	
	R. catesbeiana	*B. marinus*
σ_x	0.0118 ± 0.0012	0.0131 ± 0.0014
σ_y	0.0022 ± 0.0003	0.0040 ± 0.0001
σ_z	0.0042 ± 0.0004	0.0049 ± 0.0005

Values are means ± standard deviation.

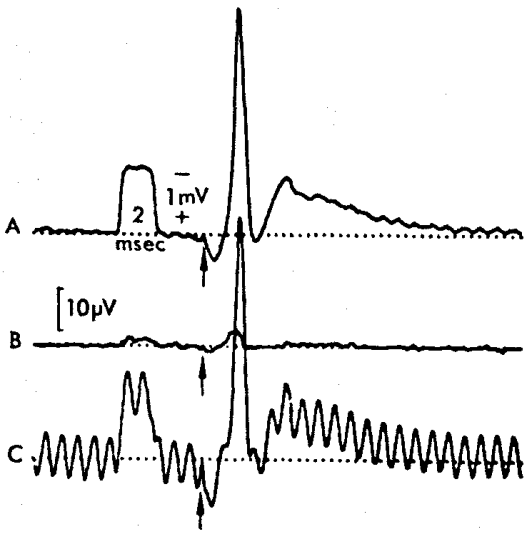

FIG. 8. Voltage dependence of conductivity. *A:* notch filter output, showing typical field potential generated by local stimulation of the folial surface (parallel fiber-induced response). *B:* resonance filter output (gain × 100). The small deflection during the peak voltage transient (seen in *A*) represents a less than 1% change in conductivity during electrical activity generated by the tissue. *C:* headstage output, consisting of parallel fiber response superimposed on potential generated by 1,000-Hz excitation sinusoidal current delivered through a second microelectrode 100 μm away. Voltage calibration same for *A* and *C*; time calibration same for all records. See METHODS and text for further details.

no significant change of conductivity was observed during field potentials generated in response to stimulation of the cerebellar parallel fibers, white matter (antidromic response), or the VIIIth nerve.

It is thus concluded that the anuran cerebellum is a homogeneous, anisotropic, ohmic medium within the electrical frequency range encountered during normal physiological activity.

DISCUSSION

The technique described in this paper is based on the use of *equation 6* to calculate the CSD from the measured field-potential distribution. *Equation 6* is derived from the set of macroscopic electrodynamic *equations 3–5* which implies that the variables are continuous functions of space. Neuronal elements are discrete structures but the use of a continuous formalism can be justified on the empirical basis that such a formalism leads to accurate predictions about the relationships between a given CSD and field potentials (21, 22). It is also apparent that the present formulation leads to a correct interpretation of the model experiment depicted in Fig. 5 where the sources and sinks are generated by discrete micropipettes.

A major reason for the success of the macroscopic equations is that CSD analysis is based on measurements which are spaced 20–100 μm apart (see ref 2), and thus the spatial resolution cannot exceed this limit. If it were possible to increase spatial resolution indefinitely, a point would be reached where the continuous assumption was invalid. The assumption would break down in two stages. First the Poisson equation formulation of a continuous distribution of sources and sinks would have to be replaced by a Laplace equation with highly complex boundary conditions described on the exterior boundaries of the neuronal elements. The Laplace equation would still represent macroscopic electrodynamics and would presumably become appropriate as resolution approached the dimensions of neuronal elements, perhaps of the order of 5–10 μm. As resolution increased even further, a second point would be reached where the basic macroscopic equations would fail and it would be necessary to consider individual ion movements; that is, to recast the problem in terms of microscopic parameters.

The present measurements, as well as those made earlier on the anuran cerebellum (3) and other tissues (26, 28), indicate that tissue impedance is not frequency dependent at the low frequencies encountered in field-potential measurements, hence membrane capacity does not contribute appreciably to extracellular impedance. Moreover, we have shown that the extracellular impedance is not potential dependent, thus the extracellular medium may be considered to be purely ohmic. The conductivity enters *equation 6* as a tensor. Thermodynamic arguments (14) indicate that this tensor is symmetric, thus there exist principal axes in which the tensor reduces to three principal components. In the cerebellum the natural rectangular coordinate system should represent these principal axes (13). Measurements demonstrate that the anuran cerebellum is anisotropic with three distinct

values of conductivity.[2] Bianisotropic tissues have been reported in the sciatic nerve of the frog (31), the dorsal column of the cat (28), and the fiber tract of the internal capsule in the cat (23). In other cases only a single value for conductivity has been reported (13, 27, 32). In some cases the technique only permitted the measurement of one component of conductivity (4, 5), and thus the degree of anisotropy could not be assessed.

Our measurements have demonstrated that the anuran cerebellum is homogeneous to a depth 300 μm, that is no appreciable conductivity gradients exist. This simplifies CSD analysis by permitting the use of *equation 11*. In other tissues inhomogeneity has been detected (7, 24) (note that these latter authors use the term anisotropy where we use inhomogeneity).

The tensorial nature of the conductivity implies that if analysis is not made in the principal axes a more complicated equation, *A8* (APPENDIX III) must be used. The reason for this is that rotation of the coordinates introduces off-diagonal elements into the conductivity tensor (regarded as a 3 x 3 matrix) resulting in additional terms involving second-order cross derivatives (see APPENDIX III). If these terms were to be neglected, spurious sources and sinks would be computed. Thus care must be taken to correctly align the measuring system with the intrinsic tissue coordinate system.

A final point regarding coordinates should be noted. *Equation 6* is expressed in vector notation and is independent of any coordinate system. Any curvilinear system could be utilized; in practice, an orthogonal system would usually be chosen which corresponded with intrinsic anatomical geometry. In the present case we have chosen a rectangular system, but for some tissues, cylindrical or spherical coordinates may be more appropriate.

We have shown that, in general, it is necessary to measure all three second-derivative components of $\nabla^2\phi$ in order to compute the CSD. Of course, if the medium is anisotropic and one or two of the components of the conductivity tensor are much less than the others, then it may be justifiable to neglect measurements in one or two axes, provided that large second derivatives do not occur in these axes. These questions can only be resolved, however, by experimental measurement of all three components of σ and of the appropriate second derivatives.

Recently it has been suggested that measurement of current flow in the z direction is sufficient for the analysis of sources and sinks of currents within the cerebellum under certain conditions (13). In general this will not be correct. First, current flow is usually three dimensional and cases of strictly one-dimensional current flow would need explicit experimental demonstration. Second, it is clear from *equation 3* that the magnitude of the source or sink of current at any given point is equal to the divergence of the current flow ($\nabla \cdot \mathbf{J}$). The divergence is not readily estimated from inspection of current flow versus time records at discrete points. In particular, even if all current flow is restricted to one dimension, a change in sign in the direction of current flow only indicates a nonzero divergence at that point and, hence, that a source or sink exists. Such a sign change does not imply that the source or sink is either a maximum or minimum or that it is localized at that point. If the current flow is three-dimensional, a sign change has little meaning since it may either be caused by the presence of a source or sink or simply by a change in direction of the current flow vector. For these reasons we believe that three-dimensional CSD analysis is the only reliable method of deriving the magnitude and location of sources and sinks from the field-potential distribution.

SUMMARY

The theoretical basis of current source-density (CSD) analysis in the central nervous system is described. Equations relating the CSD, the current flow vector, and the extracellular field potential are given. It is shown that the CSD provides superior resolution of neuronal events when compared to conventional field-potential analysis. Expressions for the CSD in rectangular Cartesian

[2] A recent paper by M. Yedlin, H. Kwan, J. T. Murphy, H. Nguyen-Huu, and Y. C. Wong, entitled "Electrical conductivity in cat cerebellar cortex" (*Exptl. Neurol.* 43: 555–569, 1974) shows that the conductivity tensor for the cat cerebellum has the same order of magnitude as that reported here for the anuran.

coordinates are derived, including the general case of anisotropic, inhomogeneous conductive tissue, and a coordinate system rotated with respect to the principal axes (APPENDIX). The minimum number of spatial dimensions for accurate CSD analysis is discussed.

The conductivity tensor was experimentally measured in frog and toad cerebella. All three principal components of the tensor were evaluated and their spatial gradients determined to be negligible. It was also shown that the conductivity was independent of potential. Thus the anuran cerebellum is anisotropic, homogeneous, and ohmic. On the basis of these results the appropriate mathematical expression for the CSD was selected.

APPENDIX I

Relationship between CSD and transmembrane current flow for simple ensemble of neuronal elements

Equation 7 of this paper defines the most general relationship between the CSD and the transmembrane current for a given neuronal element. If all the neuronal elements within a given volume are similar and are core conductors oriented normally to a given plane, then the equation takes a simple form. Let there be $\nu(x)$ elements passing normally through a unit plane area. An area A, parallel to the given plane and elementary displacement Δr, perpendicular to the plane of the area, constitutes an elementary volume $\Delta V \equiv A\Delta r$ within which $I_m(x)$ remains constant, thus the left-hand side of *equation 7* becomes $I_m(x)A\Delta r$. Within the volume ΔV there are $\nu(x)A$ core conductors with normal current $i_m(x)$ per unit surface area, where $i_m(x)$ is the transmembrane current defined by cable theory (33). The length of each core conductor within ΔV is Δr, hence the right-hand side of *equation 7* is $\nu(x)Ai_m(x)\Delta r$. Equating both sides of the equation:

$$I_m(x) = \nu(x)i_m(x) \qquad (8)$$

In cases where the core conductors are sufficiently well organized, e.g., the cerebellar parallel fibers or Purkinje cells, $\nu(x)$ may be estimated from appropriate histological material.

APPENDIX II

Simple cylindrical population of neuronal elements

A cylindrical neuronal population has a height L and diameter b (Fig. 9). Coordinates are defined relative to cylindrical axes r, θ, z and letting

$$x = r\cos\theta, y = r\sin\theta, z = z$$

equation 11 may be transformed to:

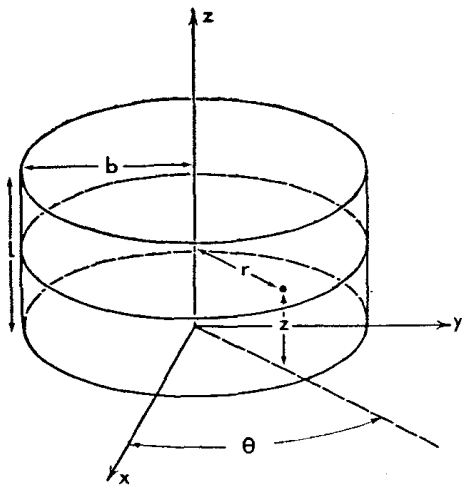

FIG. 9. Cylindrical neuronal population. Neuronal elements which supply sources and sinks of current are embedded within an infinite homogeneous conductive matrix of conductivity σ. Geometry of system referred to cylindrical polar coordinates r, θ, z. Height of cylindrical population, L and radius, b.

$$\frac{\partial^2\phi}{\partial r^2} + \frac{1}{r}\frac{\partial\phi}{\partial r} + \frac{1}{r^2}\frac{\partial^2\phi}{\partial\theta^2} + \frac{\partial^2\phi}{\partial z^2} = -\frac{I_m(z)}{\sigma} \qquad (A1)$$

for the isotropic conductivity case.

Let the CSD distribution be

$$I_m = +1 \quad 0 < z < 0.75L \quad 0 < r < b$$
$$= -3 \quad 0.75L < z < L \quad 0 < r < b$$
$$= \text{otherwise}$$

Since ϕ will not be a function of θ under those conditions, *equation A1* may be solved for $r = 0$ (the z axis) to yield (22):

$$\phi(0,z) = (1/2\sigma)\int_0^L \{[(z-z')^2 + b^2]^{\frac{1}{2}} - |z-z'|\}\, I_m(z')dz' \qquad (A2)$$

Using the identities (15)

$$g(z-z') \equiv \frac{\partial}{\partial z}|z-z'| = 1 \quad \text{for } z > z'$$
$$= -1 \quad \text{for } z < z'$$

and

$$\frac{\partial^2}{\partial z^2}|z-z'| = 2\delta(z-z')$$

where $\delta(z-z')$ is the Dirac delta function, one can derive

$$J_{z|0} = -\sigma\frac{\partial}{\partial z}\phi(0,z) = -\tfrac{1}{2}\int_0^L \{(z-z')[(z-z')^2 + b^2]^{-\frac{1}{2}} - g(z-z')\}\, I_m(z')dz' \qquad (A3)$$

and

$$\left.\frac{\partial^2\phi}{\partial z^2}\right|_{r=0} = (b^2/2\sigma)\int_0^L \{(z-z')^2 + b^2\}^{-3/2} I_m(z')dz' - I_m(z)/\sigma \quad (A4)$$

With the definition of I_m given above, the graphs depicted in Figs. 4 and 6 may be computed from *expressions A2, A3,* and *A4*.

Note that the radial component of the CSD, $Dr = (\partial^2\phi/\partial r^2) + (1/r)(\partial\phi/\partial r)$ may be computed from the relationship $Dr = -(I_m(z)/\sigma) - (\partial^2\phi/\partial z^2)$. It may be shown that, for the axis of symmetry Dr does not vanish unless $b \to \infty$, confirming that a large synchronous neuronal population is necessary for an accurate representation of the CSD using only $\partial^2\phi/\partial z^2$.

APPENDIX III

General expression for CSD with rotated Cartesian coordinates in an inhomogeneous, anisotropic medium

Denote quantities referred to the principal axes by unprimed variables and those referred to the rotated axes by primed variables. *Equation 10* is in the form of a divergence of the vector quantity J where $\mathbf{J} = -\sigma\nabla\phi$, hence *equation 10* must be invariant under rotation (30) and must have the same form in both the principal and rotated systems. Thus *equation 10* may be written as

$$\frac{\partial}{\partial x'_i}\sigma'_{ij}\frac{\partial}{\partial x'_j}\phi = \frac{\partial}{\partial x_l}\sigma_{ln}\frac{\partial}{\partial x_n}\phi = -I_m \quad (A5)$$

where repeated indices imply summation from *3* to *5*. In practice σ_{ln} is known but not σ'_{ij}. Expanding the left-hand side of *A5* one obtains:

$$\frac{\partial\sigma'_{ij}}{\partial x'_i}\cdot\frac{\partial\phi}{\partial x'_j} + \sigma'_{ij}\frac{\partial^2\phi}{\partial x'_i\partial x'_j} = -I_m \quad (A6)$$

Also $x'_i = a_{ij}x_j$ and a_{ij} is the rotation tensor (30) and σ'_{ij} must transform as a tensor under rotation, hence $\sigma'_{ij} = a_{il}a_{jn}\sigma_{ln}$ (30). Furthermore since a_{ij} is a rotation, $a_{ij}a_{ik} = \delta_{jk}$ where δ_{jk} is the Kroneker delta (30). Using these facts *equation A6* becomes:

$$a_{jn}\frac{\partial\sigma_{ln}}{\partial x_l}\frac{\partial\phi}{\partial x'_j} + a_{il}a_{jn}\sigma_{ln}\frac{\partial^2\phi}{\partial x'_i\partial x'_j} = -I_m \quad (A7)$$

In addition σ_{ln} is the conductivity tensor in the principal axes, hence it has the form $\sigma_{ln}\delta_{ln}$. Thus *A7* reduces to:

$$a_{jl}\frac{\partial\sigma_{ll}}{\partial x_l}\cdot\frac{\partial\phi}{\partial x'_j} + a_{il}a_{jl}\sigma_{ll}\frac{\partial^2\phi}{\partial x'_i\partial x'_j} = -I_m \quad (A8)$$

The general form of the rotation tensor may be expressed as a 3 x 3 matrix of the form (11);

$$a_{ij} = \delta_{ij}\cos\omega + \begin{bmatrix} C_1^2, & C_1C_2, & C_1C_3 \\ C_2C_1, & C_2^2, & C_2C_3 \\ C_3C_1, & C_3C_2, & C_3^2 \end{bmatrix}(1-\cos\omega) + \begin{bmatrix} 0, & -C_3, & C_2 \\ C_3, & 0, & -C_1 \\ -C_2, & C_1, & 0 \end{bmatrix}\sin\omega$$

where C_1, C_2, C_3 are the direction cosines of the axis of rotation with respect to the principal axes and ω is the angle of rotation.

Equation A8 thus represents the most general expression for the CSD in rectangular Cartesian coordinate. If the medium is homogeneous, $\partial\sigma_{ll}/\partial x_l = 0$, if it is isotropic, $\sigma_{ll} = \sigma$; and if the measuring axes are the principal axes, $a_{mn} = \delta_{mn}$.

ACKNOWLEDGMENTS

We are indebted to Dr. R. Llinás for his encouragement during this project and to Dr. J. Stone for his participation in the early phase of the work.

Research was supported by Public Health Service Grants NS-09916 to C. Nicholson and E-40117 to J. A. Freeman.

REFERENCES

1. Freeman, J. A. An electronic stimulus artefact suppressor. *Electroencephalog. Clin. Neurophysiol.* 31: 170–172, 1971.
2. Freeman, J. A. and Nicholson, C. Experimental optimization of current source-density technique for anuran cerebellum. *J. Neurophysiol.* 38: 369–382, 1975.
3. Freeman, J. A. and Stone, J. A technique for current density analysis of field potentials and its application to the frog cerebellum. In: *Neurobiology of Cerebellar Evolution and Development,* edited by R. Llinás. Chicago: Am. Med. Assoc., 1969, p. 421–430.
4. Freygang, W. H., Jr. and Landau, W. M. Some relations between resistivity and electrical activity in the cerebral cortex of the cat. *J. Cellular Comp. Physiol.* 45: 377–392, 1955.
5. Haberly, L. B. and Shepherd, G. M. Current-density analysis of summed evoked potentials in opossum prepyriform cortex. *J. Neurophysiol.* 36: 789–803, 1973.
6. Hagins, W. A. Electrical signs of information flow in photoreceptors. *Cold Spring Harbor Symp. Quant. Biol.* 30: 403–418, 1965.
7. Hagins, W. A., Penn, R. D., and Yoshikami, S. Dark currents and photocurrent in retinal rods. *Biophys. J.* 10: 380–412, 1970.
8. Hillman, D. E. Morphological organization of frog cerebellar cortex: a light and electron microscopic study. *J. Neurophysiol.* 32: 818–846, 1969.
9. Hillman, D. E. Neuronal organization of the cerebellar cortex in amphibia and reptilia. In: *Neurobiology of Cerebellar Evolution and Development,* edited by R. Llinás. Chicago: Am. Med. Assoc., 1969, p. 279–325.
10. Howland, B., Lettvin, J. Y., McCulloch, W. S., Pitts, W., and Wall, P. D. Reflex inhibition

by dorsal root interaction. *J. Neurophysiol.* 18: 1–17, 1955.

11. KORN, G. A. AND KORN, T. M. *Mathematical Handbook for Scientists and Engineers.* New York: McGraw, 1968.
12. KORNACKER, K. Some properties of the afferent pathway in the frog corneal reflex. *Exptl. Neurol.* 7: 224–239, 1963.
13. KWAN, H. C. AND MURPHY, J. T. A basis for extracellular current density analysis in cerebellar cortex. *J. Neurophysiol.* 37: 170–180, 1974.
14. LANDAU, L. D. AND LIFSHITZ, E. M. *Electrodynamics of Continuous Media.* Reading, Mass.: Addison-Wesley, 1960.
15. LIGHTHILL, M. J. *Introduction to Fourier Analysis and Generalised Functions.* Cambridge: Cambridge Univ. Press, 1964.
16. LLINÁS, R., BLOEDEL, J. R., AND HILLMAN, D. E. Functional characterization of neuronal circuitry of frog cerebellar cortex. *J. Neurophysiol.* 32: 847–870, 1969.
17. LLINÁS, R. AND NICHOLSON, C. Electrophysiological analysis of alligator cerebellar cortex: a study on dendritic spikes. In: *Neurobiology of Cerebellar Evolution and Development,* edited by R. Llinás. Chicago: Am. Med. Assoc., 1969, p. 431–465.
18. LLINÁS, R. AND NICHOLSON, C. Analysis of field potentials in the central nervous system. In: *Handbook of Electroencephalography and Clinical Neurophysiology,* edited by C. F. Stevens. Amsterdam: Elsevier, 1974, vol. 2, part B, p. 61–83.
19. MAXWELL, J. C. *A Treatise on Electricity and Magnetism.* New York: Dover, 1954, vol. I.
20. MORSE, P. M. AND FESHBACH, H. *Methods of Theoretical Physics.* New York: McGraw, 1963.
21. NICHOLSON, C. Theoretical analysis of field potentials in anisotropic ensembles of neuronal elements. *IEEE Trans. Biomed. Eng.* 20: 278–288, 1973.
22. NICHOLSON, C. AND LLINÁS, R. Field potentials in the alligator cerebellum and theory of their relationship to Purkinje cell dendritic spikes. *J. Neurophysiol.* 34: 509–531, 1971.
23. NICHOLSON, P. W. Specific impedance of cerebral white matter. *Exptl. Neurol.* 13: 386–401, 1965.
24. OGDEN, T. E. AND ITO, M. Avian retina. II. An evaluation of retinal electrical anisotropy. *J. Neurophysiol.* 34: 367–373, 1971.
25. PITTS, W. Investigations on synaptic transmission. In: *Cybernetics, Trans. 9th Conf.,* edited by H. von Foerster. New York: Josiah Macy, 1952, p. 159–162.
26. PLONSEY, R. AND HEPPNER, D. B. Considerations of quasistationarity in electrophysiological systems. *Bull. Math. Biophys.* 29: 657–664, 1967.
27. RANCK, J. B., JR. Specific impedance of rabbit cerebral cortex. *Exptl. Neurol.* 7: 144–152, 1963.
28. RANCK, J. B., JR., AND BEMENT, S. L. The specific impedance of the dorsal columns of cat: an anisotropic medium. *Exptl. Neurol.* 11: 451–463, 1965.
29. STONE, J. AND FREEMAN, J. A. Synaptic organisation of pigeon's optic tectum: a Golgi and current source-density analysis. *Brain Res.* 27: 203–221, 1971.
30. STRATTON, J. A. *Electromagnetic Theory.* New York: McGraw, 1941.
31. TASAKI, I. A new measurement of action currents developed by single nodes of Ranvier. *J. Neurophysiol.* 27: 1199–1206, 1964.
32. VAN HARREVELD, A., MURPHY, T., AND NOBLE, K. W. Specific impedance of rabbit's cortical tissue. *Am. J. Physiol.* 205: 203–207, 1963.
33. TAYLOR, R. E. Cable theory. In: *Physical Techniques in Biological Research. Vol. VI. Electrophysiological Methods, Part B,* edited by W. L. Nastuk. New York: Academic, 1962.
34. VUREK, G. C., BENNETT, C. M., JAMISON, R. L., AND TROY, J. L. An air-driven micropipette sharpener. *J. Appl. Physiol.* 22: 191–192, 1967.